Vol. 31 · No. 11 · November 2014

Particle & Particle Systems Characterization

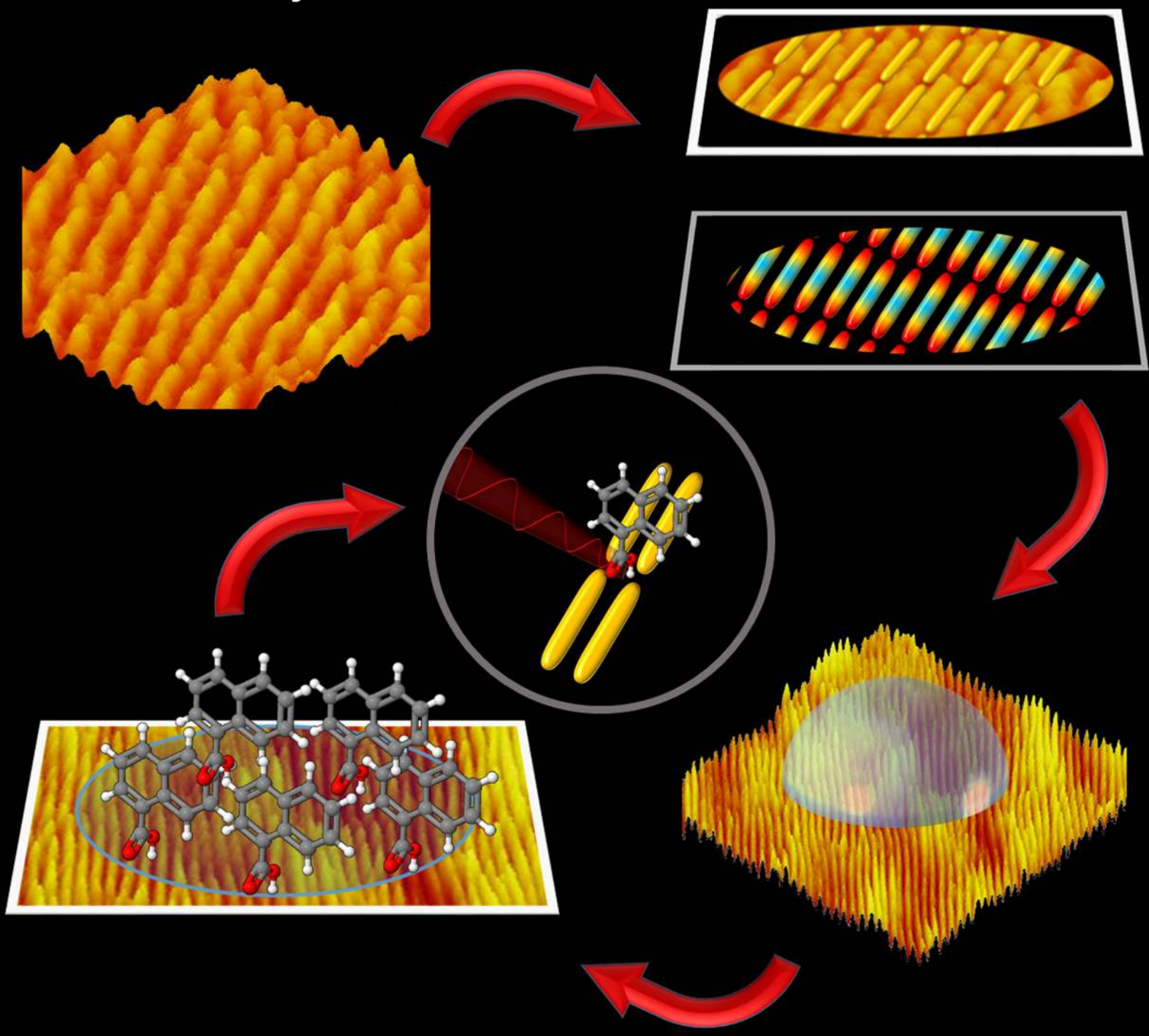

www.particle-journal.com

WILEY-VCH

Particle
& Particle Systems Characterization
www.particle-journal.com
www.MaterialsViews.com

SERS Platforms of Plasmonic Hydrophobic Surfaces for Analyte Concentration: Hierarchically Assembled Gold Nanorods on Anodized Aluminum

*Moritz Tebbe, Pavel Cherepanov, Ekaterina V. Skorb, Sergey K. Poznyak, Javier García de Abajo, Andreas Fery, Daria V. Andreeva, Ramon A. Alvarez Puebla, and Nicolas Pazos-Perez**

Efficient and homogeneous surface-enhanced Raman scattering (SERS) substrates are usually prepared using lithographic approaches, physical evaporation, or in situ chemical reduction. However, these approaches are time-consuming, expensive, and very difficult to upscale. Alternatively, template-assisted approaches using colloidal suspensions of preformed nanoparticles have become more popular because of their low cost, fast production, and ability to be scaled up easily. One of the limitations of these methods is the dimensions of the structured surfaces. In this context, a new method for designing low-cost, up-scalable surface patterns that match building block dimensionality based on anodization of aluminum, enabling a hierarchical organization of anisotropic nanoparticles, is presented. The proposed new technology starts with anodized aluminum oxide with regular parallel linear periodicities. To produce a highly efficient plasmonic surface, gold nanorods are assembled into parallel lines where the long axes of the Au rods are also oriented along the substrate lines, thus inducing reproducible tip-to-tip plasmonic coupling with the corresponding generation of highly active hotspots. Additionally, this advanced material presents an inherent hydrophobicity that can be exploited as a method for concentration of analytes on the surface. SERS detection is demonstrated with benzenethiol and 2-naphtoic acid.

1. Introduction

Surface-enhanced Raman scattering (SERS) is an ultrasensitive analytical technique with potential detection limits down to the single molecule, the possibility of multiplex analysis, and small sample preparation requirements.[1] SERS relies in the excitation of the vibrational fingerprint of the analytical target through the localized surface plasmon resonance (LSPR) generated by a plasmonic material, in close proximity to the analyte, upon illumination with a plasmon-frequency-tuned laser line.[2] Beside factors arising from the molecular structure of the probe under study or its interaction with the plasmonic material (chemical effects),[3] the intensity in SERS is extremely sensitive to the optical efficiency of the plasmonic enhancer, which is capable of amplifying the signal of extremely diluted targets against the inelastic optical background.

SERS can be achieved directly in solution or in thin films. Although SERS in solution (i.e., in colloidal dispersions of nanoparticles) represents a convenient way of analyzing certain samples,[4] thin films add versatility and can be prepared on fully portable optimal substrates that are used in a similar fashion as a reactive strip in field analysis.[5] A way of producing plasmonic thin films is by using physical methods such as physical evaporation on flat or patterned substrates.[6] Although this is an efficient method, it usually leads

M. Tebbe, P. Cherepanov, Prof. A. Fery, Dr. D. V. Andreeva, Dr. N. Pazos-Perez
Physical Chemistry II
Universität Bayreuth
Universitätsstraße 30, Bayreuth, Germany
E-mail: nicolas.pazos@uni-bayreuth.de
Dr. E. V. Skorb
Max Planck Institute of Colloids and Interfaces
Wissenschaftspark Golm
Am Mühlenberg 1, Golm 14424, Germany
Dr. E. V. Skorb, Prof. S. K. Poznyak
Chemistry Department
Belarusian State University
Leningradskaya str. 14, Minsk 220030, Belarus
Prof. J. G. de Abajo, Prof. R. A. A. Puebla
ICREA, Passeig Lluís Companys 23
08010, Barcelona, Spain
Prof. J. G. de Abajo
ICFO – The Institute of Photonic Sciences
Mediterranean Technology Park
Av. Carl Friedrich Gauss 3 08860, Castelldefels - Barcelona, Spain
Prof. R. A. A. Puebla, Dr. N. Pazos-Perez
Departamento de Quimica Fisica e Inorganica
Universitat Rovira i Virgili and Centro de Tecnologia Quimica de Cataluña
Carrer de Marcel•lí Domingo s/n 43007, Tarragona, Spain
Dr. N. Pazos-Perez
Medcom Advance, Viladecans Business Park - Edificio Brasil
Bertran i Musitu 83-85 08840, Viladecans – Barcelona, Spain

DOI: 10.1002/ppsc.201400062

© 2014 WILEY-VCH Verlag GmbH & Co. KGaA, Weinheim

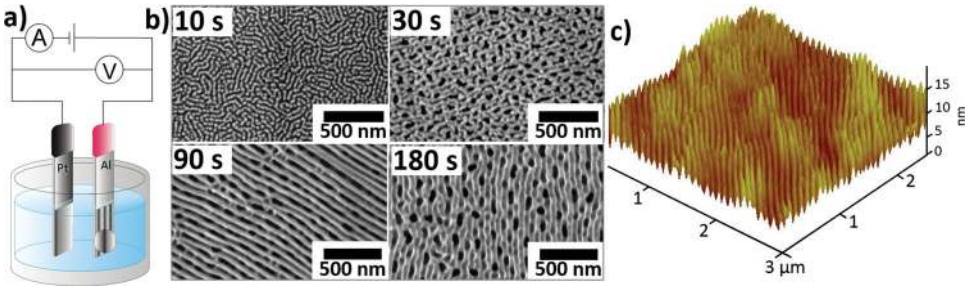

Figure 1. a) Schematic representation of the ionidized aluminum oxide (AAO) substrate preparation through galvanostatic anodization. b) Time-dependent evolution of surface morphology of aluminum substrate. c) AFM image of aluminum plate anodized for 90 s.

to rather inhomogeneous films in which plasmonic coupling takes place randomly at so-called hotspots, therefore resulting in a loss of linearity of the signal with analyte concentration.[7]

In an effort to produce geometrically homogeneous substrates, well-established lithographic approaches such as e-beam, focused-ion beam or dip-pen patterning have been proposed.[8] These approaches are however time-consuming, expensive, and very difficult to upscale. Alternatively, evaporation can be also carried out on complex surfaces such as monolayers of self-assembled polymer beads with a subsequent treatment to remove the polymer (i.e., nanosphere lithography).[9] In this case, the resulting material presents homogeneous patterned features with controlled dimensions and localized surface plasmon resonances (LSPRs). However, this method leads to large nanostructured features (over hundreds of nanometers) and is rather constrained to the few obtainable shapes and dispositions.[10] Alternatively, optical thin films can be also produced by in-situ chemical reduction of metallic salts on polymers or even using colloidal suspensions of preformed nanoparticles with their posterior retention on the desired surface by self-assembly,[11] Langmuir-Blodgett[12] or layer-by-layer methodologies.[13] Both methods present a low degree of control on the position of the nanoparticles, which yields materials with similar drawbacks to those obtained by physical evaporation.

During the last years, the development of routes to organize particles down to the nanometer scale has significantly improved. Recently, our groups developed new methodologies for the fabrication of homogeneous and efficient plasmonic surfaces for SERS, including supercrystals and organized lines of particles.[14] Specifically, nanoparticle line imprinting using wrinkles as templates has some advantages over other approaches. It is easily up scalable, inexpensive, and highly efficient. The main limitation for nanoparticle assembly using template-assisted methods is the texture size of the structured surface that is employed. As for bottom-up assembly approaches, the dimensions of the structures and the building blocks have to match. This implies that the features of the template require dimensions within the nanometer scale.

Anodized aluminum[15] surfaces emerge as good alternatives to the above-mentioned methodologies. In general, these materials consist of a packed array of hexagonal columnar cells with central, cylindrical, uniformly sized holes ranging from 4 to 200 nm in diameter with inter-hole distances between 50 and 500 nm.[16] The geometrical characteristics make of these self-ordered structures a very exciting alternative material for organization of nanoparticles. Additionally, anodized aluminum presents a natural hydrophobicity that may favor the spontaneous concentration of the target analyte onto the plasmonic surface. In this work, we suggest a new pathway to design low-cost, up-scalable surface patterns based on anodization of aluminum (Al), which match template and building block dimensionality, enabling a hierarchical organization of anisotropic nanoparticles. Moreover, the proposed new technological approach shows the unprecedented formation of a periodic linear parallel array nanostructure on the surface of anodized aluminum oxide (AAO). This structure enables the organization of Au NRs and due to its hydrophobic nature, creates a SERS substrate capable of concentrating an analyte deposited from solution increasing its sensitivity.

2. Results and Discussion

A schematic representation of the electrochemical cell for AAO formation with platinum and aluminum electrodes immersed in the electrolyte is shown in **Figure 1**a. The mechanism of pore formation in AAO is based on two processes: dissolution and growth of aluminum oxide. The diameter, length, and arrangement of the pores depend on the electrolyte used, the applied voltage, the current density, the reaction time, and the temperature.[17] Consequently, the morphology of the final AAO can be tuned by adjusting the preparation conditions. In the present work, porous AAO templates were prepared via electrochemical oxidation of aluminum in phosphoric acid solutions under galvanostatic regime. As aluminum anodization is a time-dependent process, a study of the temporal evolution of the obtained structure was carried out. Figure 1b shows SEM images of AAO revealing different structures after anodization times of 10, 30, 90, and 180 s. After 10 s, we observed formation of the hillock-like surface morphology,[18,19] followed by formation of the porous surface after 30 s. The grooved morphology reveals after 90 s of modification, finally converting into the cell-like surface morphology of the used template.

The mechanism formation of this peculiar hillock-like surface morphology can be explained in a similar way to that already described for porous AAO.[20] Briefly, upon the initiation of the anodization process, a constant current was applied and a nonconductive layer of aluminum oxide start to grow, and associated with it the anodizing voltage increases. Thus, the phosphate ions present in the working electrolyte incorporate into the AAO crystal structure. This incorporation takes place by replacing oxygen atoms on the surface of aluminum causing

© 2014 WILEY-VCH Verlag GmbH & Co. KGaA, Weinheim

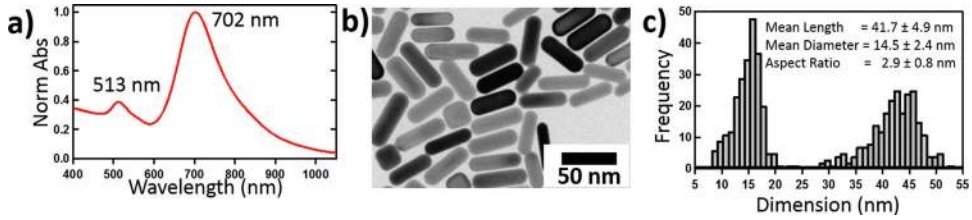

Figure 2. a) UV–vis–NIR spectrum, b) TEM image, and c) size distribution histograms of the prepared gold nanorods (GNRs).

the formation of hillocks [Figure 1b (10 s)].[18] With longer (>30 s) anodization times, a further transformation into porous AAO occurs (Figure 1b). For our purpose, the periodically grooved AAO structure (see Figure 1b, 90 s) is the most interesting one. Accordingly, the current density and anodization time were tuned in order to up scale the process for the formation of a grooved template after relatively short times. For this purpose, we adjusted the applied current density to a value of 16 mA cm^{-2}, allowing the preparation of a grooved template in 90 s. The resulting periodically grooved template exhibited a mean groove width of 36 nm (Figure 1c). Although parallel aligned pores with controllable size has been previously described,[20] the formation of periodically grooved AAO surfaces with periodicities in the nanometer regime has not been reported to the best of our knowledge. The generation of such structures could be explained by a voltage change during the anodization process. The application of a constant current implies that as the nonconductive layer of aluminum oxide grows, the resistance changes and produces a reduction in the voltage. The merging of newly formed hillocks occurs in lateral directions, forming well-pronounced corrugated morphologies of the AAO layer. Further continuation of anodization induces the formed grooves to merge with each other to reestablish a porous morphology (Figure 1b, 180 s). Consequently, the competing processes of oxide layer creation and metal dissolution[21] lead to the formation of variety of different AAO morphologies.

The linear features formed on AAO are ideal substrates on which to arrange gold nanorods (GNRs) and have those interacting in close tip-to-tip proximity. Among the plasmonic properties and applications of these particles,[22] GNRs are known to generate extremely efficient plasmon coupling when interacting tip-to-tip.[23] Therefore, we chose these particles as the plasmonic material to generate a densely populated surface of highly active hotspots. GNRs were prepared to match the size of the structures (36 nm mean groove width) by using the Murphy method,[24] with cetyltrimethylammonium bromide (CTAB) as stabilizer and Ag(I) to induce rod-like growth along the single crystalline facets of the seed particle. **Figure 2** shows GNRs of ≈42 nm in length with a thickness of ≈15 nm (aspect ratio of ≈3) exhibiting LSPRs at 513 and 702 nm, corresponding to their transversal and longitudinal modes, respectively. In order to organize the particles onto the template, a concentrated solution of GNRs was first centrifuged to decrease the amount of free CTAB and avoid the crystallization of the surfactant in the pores, and then spin-coated onto the template (**Figure 3**a) using a suitable spin speed and concentrations of CTAB and particles. The matching of particle size and nanoscale surface topography is critical to generate macroscopic hierarchical structures of anisotropic particles by bottom-up template-assisted self-assembly. Besides, the compatible wettability of the nanostructure surface with the particle solution is responsible for successful particle organization using spin coating. The latter is a well-established method of material deposition based on centrifugal forces and evaporation of the residual solvent.[25] Upon evaporation of the solvent on the nanostructured surfaces, capillary forces drag the nanoparticles into the cavities, assembling them in a close packed arrangement because of the Rayleigh instabilities and the preceding solvent front along the alumina grooves and inside the pores.[26]

The contact angle of a drop of water on the unmodified alumina is 79°. For porous surfaces, their wettability increases as a function of pore size. The contact angle for the used substrate was measured to be 104° (Figure 3b) for a mean pore size of 36 nm (estimated by PSD analysis of the AFM images).[27] The nanostructured surface thus becomes more hydrophobic after modification, in good agreement with the modified Laplace model or the capillarity and line-tension model for AAO.[28] For spin coating, we need to provide the surfaces with

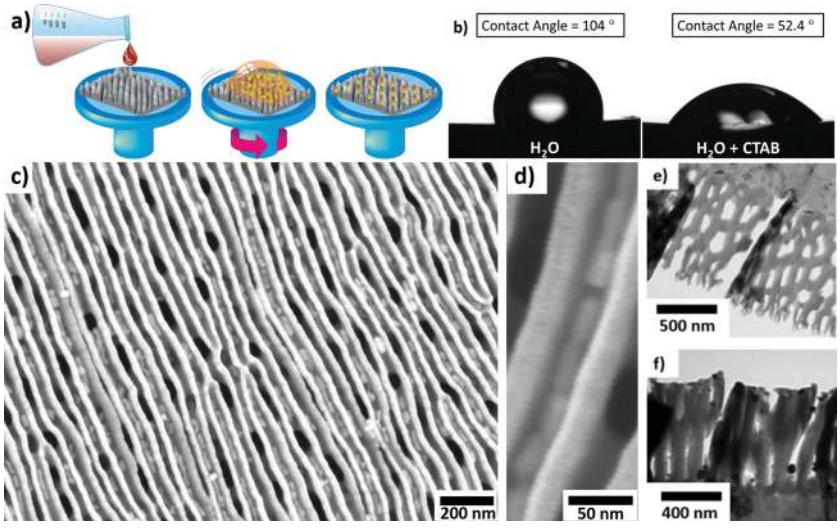

Figure 3. a) Scheme illustrating the organization of GNRs on the AAO template. b) Wettability of AAO for pure water and water solution of CTAB. c,d) SEM images of the GNRs organized onto the AAO template at different magnifications. e,f) TEM images of the microtomed template (e) before and (f) after GNRs organization.

© 2014 WILEY-VCH Verlag GmbH & Co. KGaA, Weinheim

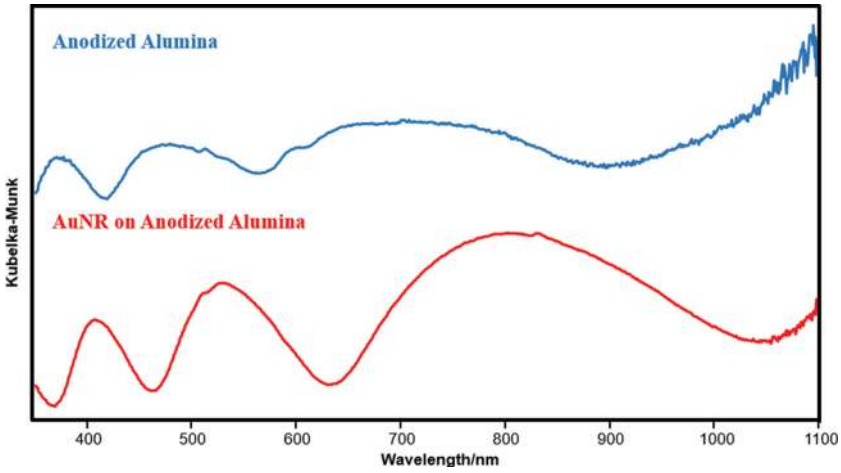

Figure 4. UV–vis–NIR reflectance spectra of the AAO template before and after the GNR organization. Both measurements were made at 60°.

adequate wettability. The aqueous suspensions of GNRs stabilized by CTAB have a surface tension of 35 mN m^{-1} (above critical micelle concentration of CTAB).[29] At the same time, the contact angle between the used solution containing CTAB and the AAO was 52.4°. Consequently, CTAB provided the enhanced wettability of the nanostructured alumina substrate. Figure 3c,d shows that GNRs are linearly aligned inside the grooves. We stress again that the observed preferential organization along the long axes of the rods (Figure 3c,d) is achieved because of the chosen sizes of the rods (42 × 15 nm) and the width of the grooves (36 nm). Furthermore, we observe the presence of darker spots within these grooves, corresponding to pores of the anodized surface. The TEM images of the ultramicrotomed surfaces before (Figure 3e) and after (Figure 3f) particle deposition reveals the presence of GNRs inside both grooves and pores.

Optical reflectance spectroscopy of the Au nanorod arrays supported in AAO matrix reveals an interference pattern with several features in the UV-Vis-NIR region (see **Figure 4**). The interferometric signals are shifted toward longer wavelengths when Au rods are present, this effect arise from a modulation of the local dielectric causing a shift in signals[30] and, can be related to a change of the effective optical thickness (product of thickness and refractive index),[31] which is attributed to a change in the refractive index of the layer medium when Au rods are present.[30,32]

Although there is a high density of AuNRs on AAO substrates that are aligned along the surface indentations, their plasmonic resonances are sensitive to variations in their geometrical dimensions, as well as to the gap distances between contiguous rods (see **Figure 5**). Additionally, these plasmons are generally expected to lie below 700 nm light wavelength (Figure 2a,b), and therefore, they cannot be directly excited neither by the 785 nm laser light nor by the emitted inelastic signal at even larger wavelengths. However, the gap geometry leads to large field enhancements near the surface even at lower photon energies due to non-resonant plasmon polarization, thus contributing to a substantial SERS enhancement, as shown in Figure 5c. The actual value of the enhancement depends on the specific gap separations. In our samples, we expect to have a distribution of separations of the order of a few nanometers down to touching. The effect of the substrate is not contemplated in the calculations shown in Figure 5, but as already mentioned the substrate will have a strong influence on the dielectric environment and will lead to a substantial redshift of the spectra similar to the simulations shown in Figure 5a,c for rods in water compared with air. Furthermore, the tip-to-tip dimer configuration may also lead to a further red shift as depicted in Figure 5a,b. Thus, both effects will lead to a larger SERS enhancement because of a greater degree of overlap with the wavelengths of excitation of the light.

In order to test the optical efficiency of our materials for SERS, we designed an experiment involving two well-known analytes, benzenethiol (BT) and 2-naphtoic acid (NA). Furthermore, the same experiment was carried out on a commercial optical surface (Klarite) (see **Figure 6**) in order to compare the results with those obtained from a common SERS substrate. Before the analyte deposition, the plasmonic substrates were treated with oxygen plasma to eliminate residual CTAB from the plasmonic surfaces.[33] Both substrates were subsequently exposed to benzenethiol in gas phase. It is important to note that with this experimental setup the gaseous BT is adsorbed onto the entire plasmonic surfaces. Although both plasmonic substrates show clearly the vibrational pattern of BT (C–H bending at 1022 cm^{-1}, ring breathings at 1073 and 999 cm^{-1}, and ring stretching at 1570 cm^{-1}),[34] the average intensity of the obtained spectra is remarkably different, as shown in Figure 6. It is thus instructive to point out some differences between both types of samples (AAO-GNRs and Klarite). First, AAO-GNRs films provide a homogeneous signal through the entire film, which is covered with a rather homogenous density of hotspots (mainly rod ends and tip-to-tip gaps), while Klarite substrates present a high activity only in a sparse set of randomly occurring spots on the surface. The homogeneous distribution of hotspots (tip-to-tip plasmonic coupling between the rods trapped in the grooves) in our films is in clear contrast with the commercial substrate, which exhibits a characteristic random distribution of such optically high-efficient regions for evaporated films. Furthermore and importantly, our substrates provide a five-fold higher signal than provided by the best spots in the Klarite substrate.

The effect of hydrophobicity provided by the AAO-GNRs substrate after plasma cleaning of CTAB on aqueous solutions deserves further consideration. We studied it, a diluted solution of NA in water (10 µL, 10^{-5} M) was cast over both substrates and air dried. The intrinsic hydrophobicity of the alumina seems to determine the contact angle of occurring droplets in the AAO-GNRs substrates, which is similar to the one reported above (105°), with the final result of a concentration of the analyte on a small spatial region that is fully covered with plasmonic particles. In contrast, the drop contact angle in the commercial substrate was much smaller (68°), thus resulting in more diluted analyte distributions on the surface. As a consequence, although

© 2014 WILEY-VCH Verlag GmbH & Co. KGaA, Weinheim

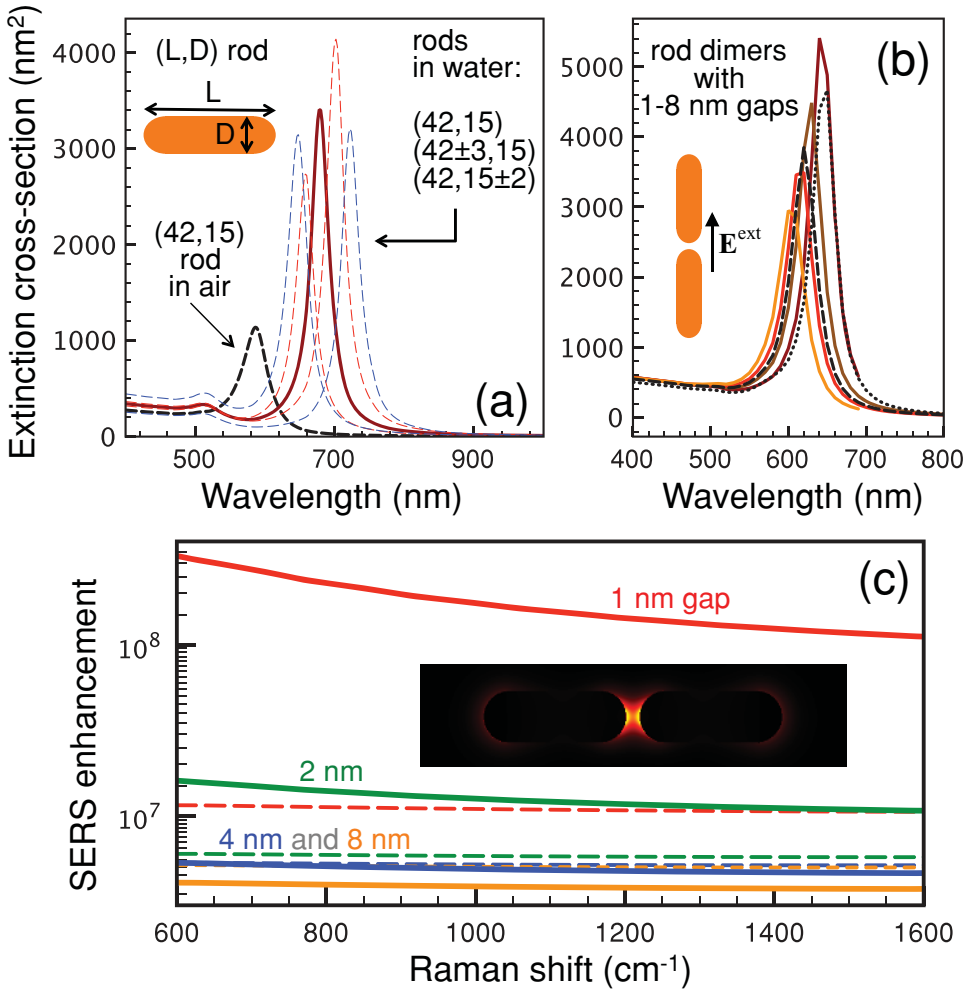

Figure 5. Optical response and SERS activity of individual and paired GNRs. a) Extinction cross-section of individual AuNRs of dimensions similar to those shown in Figure 2. The longitudinal resonance of rods in water (right curves) is considerably red-shifted with respect to airborne rods (left curves), and it is also shifted due to variations in rod dimensions, giving rise to an observed broad peak (Figure 2a). b) Optical resonance of pairs of AuNRs longitudinally aligned as observed on an AAO sample (Figure 3). A plasmon redshift accompanied by an increase in cross section is observed as the gap is narrowed down from 8 to 1 nm (solid curves). The plasmon is also sensitive to the dimensions of the rods (see dotted curve, corresponding to a (39,15)–(42,15) dimer, and dashed curve, for (42,13)–(42,15), both of them with a 2-nm gap). c) Surface-averaged SERS enhancement factors for molecules distributed 0.5 nm away from the surface of two neighboring nanorods aligned as shown in the inset of (b). The rods are assumed to be either in air (broken curves) or in water (solid curves) and illuminated with 785 nm light (a water environment might be more appropriate to describe residual humidity surrounding the rods during the SERS measurements). The enhancement is referred to the Raman signal from the same molecules away from the rods, averaged over polarizations and molecule orientations for both illumination and light collection along directions normal to the rod axes. The inset in (c) shows the near-field intensity of the gap mode in the 4-nm-gap dimer in water (linear scale saturated to 5000 times the incident field).

both surfaces show SERS activity of NA (ring stretching at 1632 and at 1388 cm^{-1}, CH bending at 1468 cm^{-1}, ring breathing at 1018 cm^{-1}, and C-H deformation at 770 cm^{-1}),[35] AAO-GNRs substrates exhibit a similar surface homogeneity to that commented above, but with an additional intensification of the SERS signal that is quantified by a 40-fold observed increase in intensity with respect to the commercial substrate.

3. Conclusion

In summary, we demonstrate a new method for the large-scale production of efficient plasmonic surfaces based on controlled organization of gold nanorods retained on AAO surfaces. We take advantage of colloid synthesis methods to prepare particles with appropriate dimensions and we use surface chemistry to retain and align them on grooved AAO substrates. This results in an abundant distribution of hotspots originating in tip-to-tip interaction between the rods, where SERS amplification is taking place. We further exploit the physical and chemical properties of the AAO surface to design an optical sensor with the ability of concentrating trace amounts of analytes in an aqueous solution, yielding further intensification of the SERS signals. This method of preparing plasmonic substrates paves the road for the fabrication of reactive-strip optical sensors that are especially suitable for field analysis in environmental

© 2014 WILEY-VCH Verlag GmbH & Co. KGaA, Weinheim

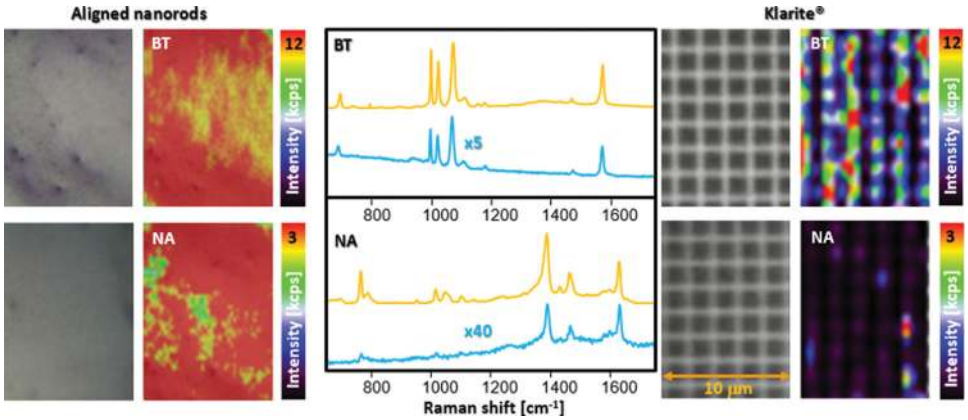

Figure 6. Optical and SERS images (left) and SERS spectra (yellow) of BT and NA in AAO-GNRs compared with the same analytes on a commercial surface Klarite (right and blue spectra).

monitoring or the design of diagnostic devices for medical applications.

4. Experimental Section

Materials: Silver nitrate (99.9999 %, $AgNO_3$), sodium borohydride (99.99 %, $NaBH_4$), gold(III) chloride trihydrate (99.9 %, $HAuCl_4{\cdot}3H_2O$), nitric acid (32.5 %, HNO_3), benzenethiol, 2-naphthoic acid, and ascorbic acid (99 %) were purchased from Sigma–Aldrich (Germany). Cetyltrimethylammonium bromide (99 %, CTAB) was obtained from Merck. All reactants were used without further purification. Mili-Q water (18 MΩ cm^{-1}) was used in all aqueous solutions, and all the glassware was cleaned with aqua regia before the experiments. High-purity Al foil of 1-mm thickness (99.997 %) supplied by Sigma–Aldrich was used as a substrate for fabrication of AAO. Phosphoric acid, perchloric acid, and ethanol were also supplied by Sigma–Aldrich (Germany) and used as received.

Preparation of AAO Substrates: Al foils were cut in rectangles (7 mm × 40 mm), cleaned with acetone, and distilled water in order to remove any residuals and then dried under dry air. After cleaning, the Al foils were electrochemically polished in a 1:4 mixture solution of 65 wt% $HClO_4$ and 96 vol% ethanol. Temperature during the polishing procedure was kept under 5 °C. Mirror-finished Al foils with exposed-to-anodization area of 3 cm^2 were used as an anode in a home-made two-electrode electrochemical cell with Pt-wire electrode serving as a cathode (distance between electrodes was set to 1 cm). The anodization process was performed in galvanostatic mode under a constant current of 16 mA cm^{-2} for time periods of 10, 30, 90, and 180 s at ambient temperature. 1.0 M H_3PO_4 was used as a working electrolyte.

Preparation of Gold Nanorods: Particles of ≈42 nm length and 15 nm width were produced by adapting an established procedure reported.[24,36] Briefly, seed particles were prepared by adding 300 µL of a 0.01 M $NaBH_4$ solution in a 5-mL mixture of 0.1 M CTAB and 0.25×10^{-3} M $HAuCl_4$ under vigorous stirring. The solution was stirred rapidly for 2 min followed by continued slow stirring. A 200 mL of a 0.1 M CTAB solution containing 0.25×10^{-3} M $HAuCl_4$, 0.04×10^{-3} M $AgNO_3$, 1.3 mL of a 0.1 M HNO_3 solution to adjust the pH, and 0.35×10^{-3} M ascorbic acid as reducing agent were prepared. 2 mL of the prepared seeds was added to this solution after 30 min of stirring. The entire solution was mixed extensively and reaction took place at 32 °C for 24 h. The particles were cleaned and concentrated via multiple centrifugation steps at 16 000 rcf for 30 min to a final gold concentration of 5 mg mL^{-1} and 7.5×10^{-3} M CTAB.

Nanorod Organization: In order to organize the particles, a solution containing Au NRs was spin-coated on the aluminum substrates, which were pasted on a glass slide as support. The most critical experimental parameters to achieve a good particle organization are the CTAB and particle concentration together with the spin speed and time. These parameters were adjusted in order to achieve the best results as follow: 20 µL of the particle solution (5 mg mL^{-1} Au and 7.5×10^{-3} M CTAB) were spin-coated at 2000 rpm for 120 s. The substrates with the deposited nanoparticles show a red color.

Characterization: UV–vis spectroscopy (PerkinElmer, Lambda 19), UV–vis reflectance spectroscopy (Analytik Jena AG, SPECORD PLUS), transmission and scanning electron microscopy (TEM, LEO 922 EFTEM operating at 200 kV and LEO 1530 FE-SEM, Zeiss, respectively) were applied to characterize the optical response, structure, and size of the nanoparticles and their arrays. AFM images were obtained using a commercial atomic force microscope (DimensionTM 3100M equipped with a Nanoscope IIIm controller, Veeco Instruments Inc., USA) operating in tapping mode. Silicon cantilevers with a force constant of typically 35–47.2 N m^{-1} (OMCL-AC160TS, Olympus, Japan, typical frequency of 303 kHz) were utilized.

SERS Characterization: Benzenethiol was adsorbed in gas phase on the whole surface of the metallic samples by casting a drop of BT (0.1 M in ethanol) in a Petri dish where the substrate was also contained. A diluted solution of naphthoic acid (10 µL, 10^{-5} M) was cast on the plasmonic surfaces and air dried. SERS spectra were collected in backscattering geometry with a Renishaw Invia Reflex system equipped with a 2D-CCD detector and a Leica confocal microscope. The spectrograph used a high-resolution grating (1200 g cm^{-1}) with additional band pass filter optics. Excitation of the sample was carried out with a 785-nm diode laser line, with acquisition times of 200 ms and power at the sample of about 1 mW, using the Renishaw's StreamLine accessory. The laser was focused onto the sample with a 50× objective providing a spatial resolution of ca. 1 µm.

Acknowledgements

M.T. and P.C. contributed equally to this work. This work was funded by the Spanish Ministerio de Economia y Competitividad (CTQ2011-23167), the European Research Council (CrossSERS, FP7MC-IEF329131, PRIOSERS FP7MC-IEF-623527, and ERC-2012-StG 306686 METAMECH), NatoCBRN collaborative project CLG 984267, the German Research Foundation (DFG) within the collaborative research center SFB 840. M.T. was supported by the Elite Network Bavaria in the frame of the Elite Study Program "Macromolecular Science" and funded via a grant for Ph.D. candidates according to Bavarian elite promotion law (BayEFG).

Received: March 25, 2014
Revised: May 6, 2014
Published online: July 2, 2014

© 2014 WILEY-VCH Verlag GmbH & Co. KGaA, Weinheim

[1] a) N. J. Halas, M. Moskovits, *MRS Bull.* **2013**, *38*, 607; b) B. Sharma, M. Fernanda Cardinal, S. L. Kleinman, N. G. Greeneltch, R. R. Frontiera, M. G. Blaber, G. C. Schatz, R. P. Van Duyne, *MRS Bull.* **2013**, *38*, 615.
[2] R. A. Álvarez-Puebla, *J. Phys. Chem. Lett.* **2012**, *3*, 857.
[3] A. Otto, *J. Raman Spectrosc.* **2005**, *36*, 497.
[4] C. Andreou, M. R. Hoonejani, M. R. Barmi, M. Moskovits, C. D. Meinhart, *ACS Nano* **2013**, *7*, 7157.
[5] R. Zhang, B. B. Xu, X. Q. Liu, Y. L. Zhang, Y. Xu, Q. D. Chen, H. B. Sun, *Chem. Commun.* **2012**, *48*, 5913.
[6] W. B. Lacy, J. M. Williams, L. A. Wenzler, T. P. Beebe Jr., J. M. Harris, *Anal. Chem.* **1996**, *68*, 1003.
[7] A. Otto, *J. Raman Spectrosc.* **2006**, *37*, 937.
[8] a) N. A. Abu Hatab, J. M. Oran, M. J. Sepaniak, *ACS Nano* **2008**, *2*, 377; b) N. L. Rosi, C. A. Mirkin, *Chem. Rev.* **2005**, *105*, 1547.
[9] B. Sharma, R. R. Frontiera, A. I. Henry, E. Ringe, R. P. Van Duyne, *Mater. Today* **2012**, *15*, 16.
[10] K. Matczyszyn, J. Olesiak-Banska, *J. Nanophotonics* **2012**, *6*, 064505.
[11] L. Guerrini, E. Pazos, C. Penas, M. E. Vázquez, J. L. Mascareñas, R. A. Alvarez-Puebla, *J. Am. Chem. Soc.* **2013**, *135*, 10314.
[12] A. Tao, F. Kim, C. Hess, J. Goldberger, R. He, Y. Sun, Y. Xia, P. Yang, *Nano Lett.* **2003**, *3*, 1229.
[13] N. P. W. Pieczonka, P. J. G. Goulet, R. F. Aroca, *J. Am. Chem. Soc.* **2006**, *128*, 12626.
[14] a) M. Alba, N. Pazos-Perez, B. Vaz, P. Formentin, M. Tebbe, M. A. Correa-Duarte, P. Granero, J. Ferré-Borrull, R. Alvarez, J. Pallares, A. Fery, A. R. De Lera, L. F. Marsal, R. A. Alvarez-Puebla, *Angew. Chem. Int. Ed.* **2013**, *52*, 6459; b) N. Pazos-Pérez, W. Ni, A. Schweikart, R. A. Alvarez-Puebla, A. Fery, L. M. Liz-Marzán, *Chem. Sci.* **2010**, *1*, 174.
[15] a) H. Masuda, K. Fukuda, *Science* **1995**, *268*, 1466; b) E. V. Skorb, D. V. Andreeva, *Adv. Funct. Mater.* **2013**, *23*, 4483.
[16] K. Nielsch, J. Choi, K. Schwirn, R. B. Wehrspohn, U. Gösele, *Nano Lett.* **2002**, *2*, 677.
[17] F. Li, L. Zhang, R. M. Metzger, *Chem. Mater.* **1998**, *10*, 2470.
[18] M. Michalska-Domańska, M. Norek, W. J. Stępniowski, B. Budner, *Electrochim. Acta* **2013**, *105*, 424.
[19] P. Chaudhar, *J. Appl. Phys.* **1974**, *45*, 4339.
[20] K. Kant, S. P. Low, A. Marshal, J. G. Shapter, D. Losic, *ACS Appl. Mater. Interfaces* **2010**, *2*, 3447.
[21] K. Rana, G. Kucukayan-Dogu, E. Bengu, *Appl. Surface Sci.* **2012**, *258*, 7112.
[22] H. Chen, L. Shao, Q. Li, J. Wang, *Chem. Soc. Rev.* **2013**, *42*, 2679.
[23] a) J. Aizpurua, G. W. Bryant, L. J. Richter, F. J. García de Abajo, B. K. Kelley, T. Mallouk, *Phys. Rev. B* **2005**, *71*, 235420; b) A. Lee, A. Ahmed, D. P. dos Santos, N. Coombs, J. I. Park, R. Gordon, A. G. Brolo, E. Kumacheva, *J. Phys. Chem. C* **2012**, *116*, 5538; b) L. Wang, Y. Zhu, L. Xu, W. Chen, H. Kuang, L. Liu, A. Agarwal, C. Xu, N. A. Kotov, *Angew. Chem. Int. Ed.* **2010**, *49*, 5472.
[24] N. R. Jana, L. Gearheart, C. J. Murphy, *J. Phys. Chem. B* **2001**, *105*, 4065.
[25] a) D. E. Bornside, C. W. Macosko, L. E. Scriven, *J. Appl. Phys.* **1989**, *66*, 5185; b) P. Colson, R. Cloots, C. Henrist, *Langmuir* **2011**, *27*, 12800.
[26] a) R. Seemann, M. Brinkmann, S. Herminghaus, K. Khare, B. M. Law, S. McBride, K. Kostourou, E. Gurevich, S. Bommer, C. Herrmann, D. Michler, *J. Phys. Condes. Matter* **2011**, *23*, 184108; b) R. Seemann, M. Brinkmann, E. J. Kramer, F. F. Lange, R. Lipowsky, *Proc. Natl. Acad. Sci. USA* **2005**, *102*, 1848.
[27] a) S. Karan, B. Mallik, *Phys. Chem. Chem. Phys.* **2008**, *10*, 6751; b) C. Xu, H. Tian, C. E. Reece, M. J. Kelley, *Phys. Rev. Special Topics - Acceler. Beams* **2012**, *15*, 043502.
[28] V. Raspal, K. O. Awitor, C. Massard, E. Feschet-Chassot, R. S. P. Bokalawela, M. B. Johnson, *Langmuir* **2012**, *28*, 11064.
[29] M. T. Yatcilla, K. L. Herrington, L. L. Brasher, E. W. Kaler, S. Chiruvolu, J. A. Zasadzinski, *J. Phys. Chem.* **1996**, *100*, 5874.
[30] D. P. Lyvers, J.-M. Moon, A. V. Kildishev, V. M. Shalaev, A. Wei, *ACS Nano* **2008**, *2*, 2569.
[31] V. S.-Y. Lin, K. Motesharei, K.-P. S. Dancil, M. J. Sailor, M. R. Ghadiri, *Science* **1997**, *278*, 840.
[32] D.-K. Kim, K. Kerman, M. Saito, R. R. Sathuluri, T. Endo, S. Yamamura, Y.-S. Kwon, E. Tamiya, *Anal. Chem.* **2007**, *79*, 1855.
[33] R. A. Alvarez-Puebla, A. Agarwal, P. Manna, B. P. Khanal, P. Aldeanueva-Potel, E. Carbó-Argibay, N. Pazos-Pérez, L. Vigderman, E. R. Zubarev, N. A. Kotov, L. M. Liz-Marzán, *Proc. Natl. Acad. Sci. USA* **2011**, *108*, 8157.
[34] N. Pazos-Perez, C. S. Wagner, J. M. Romo-Herrera, L. M. Liz-Marzán, F. J. García De Abajo, A. Wittemann, A. Fery, R. A. Alvarez-Puebla, *Angew. Chem. Int. Ed.* **2012**, *51*, 12688.
[35] R. A. Alvarez-Puebla, R. F. Aroca, *Anal. Chem.* **2009**, *81*, 2280.
[36] B. Nikoobakht, M. A. El-Sayed, *Chem. Mater.* **2003**, *15*, 1957.

© 2014 WILEY-VCH Verlag GmbH & Co. KGaA, Weinheim